Available online at www.sciencedirect.com

ScienceDirect

Nuclear Physics B 949 (2019) 114796

NUCLEAR PHYSICS B

www.elsevier.com/locate/nuclphysb

Characteristic electromagnetic waves caused by tensorial and possible nontensorial thermal high-frequency gravitational waves from magnetars

Hao Wen *, Fang-Yu Li *, Jin Li, Zhen-Yun Fang

Physics Department, Chongqing University, Chongqing 401331, China

Received 7 March 2019; received in revised form 30 August 2019; accepted 8 October 2019
Available online 11 October 2019
Editor: Hong-Jian He

Abstract

Interaction between the gravitational waves (GWs) and the strong magnetic fields would lead to the perturbed electromagnetic waves (EMWs). Magnetars can have ultra-strong surface magnetic fields $\sim 10^{11}$Tesla, and meanwhile, they would generate the thermal high-frequency GWs (HFGWs) caused by the Fermi liquid phonons and the gravitational bremsstrahlung inside. Here, we for the first time address the perturbed EMWs caused by such thermal-HFGWs interacting with the ultra-strong surface magnetic fields of the magnetars. It is expected that the perturbed EMWs would distribute in very characteristic patterns that have never been predicted before, which may deliver and reflect the crucial information of the polarizations (tensorial and possible nontensorial) of the thermal-HFGWs and the particular features of the structures of magnetars. The estimated power density of such perturbed EMWs would reach $\sim 10^6$–10^8 W/m^2 in the area around the surface of magnetar, and the strengths of perturbed EMWs in the observational direction would appear in characteristic pulse-like envelopes. Obtained results may suggest the novel effect of potential evidences of the possible nontensorial GWs, the thermal-HFGWs from magnetars, the mechanism of EM response to the GWs, and the models of magnetars and their magnetic fields.

* Corresponding authors.
E-mail addresses: wenhao@cqu.edu.cn (H. Wen), fangyuli@cqu.edu.cn (F.-Y. Li).

https://doi.org/10.1016/j.nuclphysb.2019.114796

1. Introduction

The LIGO scientific collaboration and the Virgo collaboration have so far reported 11 gravitational wave (GW) events (GW150914, GW151012, GW151226, GW170104, GW170608, GW170729, GW170809, GW170814, GW170817, GW170818, GW170823) [1–8] from binary black hole mergers [1–5,7,8] (with frequencies around 30 Hz to 450 Hz and dimensionless amplitudes $h \sim 10^{-21}$ to $\sim 10^{-22}$ near the Earth) or from binary neutron star merger [6] [GW170817, comes with the first electromagnetic (EM) counterpart]. These great discoveries inaugurated a new era of the GW Astronomy. Meanwhile, in order to obtain more extensive and in-depth astronomical information, it will also be very expected to expand the observations in broader frequency bands (low, intermediate, high, and very high-frequency bands), through a wider variety of methods with different effects, aiming on more types of sources, to explore richer information of properties of the gravity and Universe. In this case, here, we try to present a possible novel effect of the perturbed EM waves (EMWs) caused by the thermal GWs from the magnetars (in very high frequencies with tensorial and possible nontensorial polarizations) interacting with the ultra-strong magnetic fields of the magnetars.

Interactions between the GWs and the EM fields had been long widely studied [9–31], e.g., B-mode polarization in cosmic microwave background (CMB) caused by very low-frequency primordial (relic) GWs [9–13], EM response to GWs [15–31] (including the EM response to high-frequency GWs (HFGWs) which would lead to the perturbed EMWs [21–31]). For such issues, physical conditions and factors of the EM systems, such as their strengths, structures and scales, will crucially influence the effects of the perturbed EMWs caused by the GWs. Therefore, some celestial bodies with very intense EM fields, such as the magnetars, would act as natural astrophysical laboratories to provide extremely strong EM backgrounds. As a particular kind of neutron stars, magnetars can have ultra-high surface magnetic fields up to $\sim 10^{11}$Tesla, and meanwhile, the magnetars could also be the sources of the thermal-HFGWs [32–39] (generated from the thermal "zero-sound" phonons of Fermi liquid and the gravitational bremsstrahlung inside the magnetars, in very high frequencies $\sim 10^{21}$ Hz [32]). Thus, the magnetars could generate thermal-HFGWs to interact with their own ultra-strong surface magnetic fields and lead to the perturbed EMWs.

In this article, based on the electrodynamics in curved spacetime, we investigate the generation and properties of such perturbed EMWs, and the results suggest that they would have very characteristic patterns that have never been predicted before, which may deliver and reflect the particular information of the structures of the magnetar surface magnetic fields and the polarizations (including possible nontensorial ones) of the thermal-HFGWs.

In frame of general relativity (GR), GWs have only tensor polarizations ($+$ and $\times$ modes), but the generic metric theories may predict GWs with up to six polarizations (including vector modes: x, y, and scalar modes: b, l) [40,41]. The nontensorial polarizations of GWs is a crucial topic which has been widely investigated [21,42–58], but we still very lack information about the nontensorial modes of the thermal GWs produced by thermal sources inside the celestial bodies. Also, we do not know the properties of the possible components of nontensorial modes and their proportions to the tensorial GWs. Interestingly, we find that the tensorial, nontensorial, and mixed modes of the thermal-HFGWs, would lead to the perturbed EMWs in very characteristic but different manners. In this case, studying such perturbed EMWs would also be a potential window to investigate the possible nontensorial GWs.

Plan of this paper is as follows. In Sect. 2, the thermal-HFGWs from the magnetars and the employed forms of the surface magnetic fields of magnetars are presented. In Sect. 3, the

perturbed EMWs caused by the thermal-HFGWs are calculated and their characteristic properties are addressed, for both tensorial and nontensorial cases. In Sect. 4, we give the summary and discussion.

2. Thermal high-frequency gravitational waves and ultra-strong surface magnetic fields of magnetars

Magnetars, as a special type of neutron stars, would emit HFGWs from their inner thermal sources of high-energy processes, such as the "zero-sound" phonons of Fermi liquid and thermal gravitational bremsstrahlung [32]. In Ref. [32], in order to simplify the problem, the calculation of generation of the thermal GWs contributed by the "zero-sound" phonons of Fermi liquid, was partially based on some approximations, and thus here, for obtaining more conservative and safe estimations, we only include the contribution of generation of thermal GWs by the bremsstrahlung, as the starting point for this article. The luminosity of such thermal gravitational radiation (caused by bremsstrahlung only) can be expressed [32]:

$$P_{total} = \frac{4^5}{5^3}(\frac{3}{\pi})^{2/3}\frac{G}{c^5}(\frac{a}{\hbar})^2\frac{M_{NS}}{m}n^{2/3}(kT)^4. \tag{1}$$

Here m is the mass of neutron; M_{NS} is the mass of neutron star (or magnetar); "n" is the particle number density; "a" represents the neutron radius (by hard-core potential). For instance, if we take typical parameters of a magnetar, e.g., radius $\simeq 10^4$ m, $M_{NS} \simeq 1M_{\odot}$, $a \simeq 0.4 \times 10^{-15}$ m, $T \simeq 5 \times 10^{10}$ K, then the frequency of the generated thermal-HFGWs is $\sim 6.5 \times 10^{21}$ Hz, and the total power of such thermal-HFGWs is $P_{total} \sim 7.4 \times 10^{23}$ Watt. Therefore, for a simple situation, the energy flux density of thermal-HFGWs at distance of r (outside the magnetar) should be $P_{total}/4\pi r^2$, and according to the theory of Landau [59], the energy flux density of GWs is $\sim (c^3\omega^2A^2)/(8\pi G)$ [A is the dimensionless amplitude], then the amplitude of thermal-HFGWs [$A^{thm}_{+,\times,x,y}$, in this article we only consider the tensor-mode ($+$, $\times$) and the vector-mode (x, y)] at distance r can be expressed as:

$$A^{thm}_{+,\times,x,y} = \sqrt{\frac{P_{total}8\pi G}{4\pi r^2 c^3\omega^2}}. \tag{2}$$

This indicates that the amplitude decays in the same way as the spherical GWs, i.e., $\sim 1/r$. For various discovered magnetars or magnetar candidates, their parameters would vary case to case, and lots of their values are still not exactly confirmed so far. In Table 1, it presents some magnetars with possible parameters, and the corresponding frequencies and amplitudes of the thermal-HFGWs are listed. These estimated amplitudes are commonly less than $\sim 10^{-30}$ under certain conditions, but their frequencies are in very high band up to $\sim 10^{21}$ Hz, so the power fluxes of the thermal-HFGWs are still of considerable magnitudes.

On the other hand, the magnetars can have extremely strong surface magnetic fields $\sim 10^{11}$Tesla or even higher [60], whereas, so far, we are not sure about the concrete form of the surface distribution of such magnetic fields. Therefore, based on previous research [61], here we employ a typical form of magnetar surface magnetic fields:

$$\mathbf{B}^{surf} = \vec{\nabla} \times (\vec{r} \times \vec{\nabla} S), \tag{3}$$

We use the spherical coordinates with orthonormal basis of $\mathbf{e}_r$, $\mathbf{e}_\theta$ and $\mathbf{e}_\phi$; the $\mathbf{r} = r\mathbf{e}_r$, and $\mathbf{B} = B_r\mathbf{e}_r + B_\theta\mathbf{e}_\theta + B_\phi\mathbf{e}_\phi$. The scalar function S can be expanded in a series of spherical harmonics:

Table 1
Dimensionless amplitudes (around magnetars) of thermal-HFGWs emitted from magnetars by some possible parameters. The "T" denotes the temperature of thermal sources of the thermal-HFGWs inside the magnetars.

Magnetars with possible parameters	Frequency and amplitude of thermal-HFGWs
SGR 1806-20 $r \sim 12$ km, $M \sim 1.25 M_{\odot}$ $T \sim 200$ KeV	$freq. \sim 4.8 \times 10^{19}$ Hz $A^{thm} \sim 8.0 \times 10^{-34}$
Possible magnetar 1 $r \sim 10$ km, $M \sim 2 M_{\odot}$ $T \sim 500$ KeV	$freq. \sim 1.2 \times 10^{20}$ Hz $A^{thm} \sim 4.3 \times 10^{-33}$
Possible magnetar 2 $r \sim 13$ km, $M \sim 2.5 M_{\odot}$ $T \sim 5000$ KeV	$freq. \sim 1.2 \times 10^{21}$ Hz $A^{thm} \sim 3.0 \times 10^{-32}$

$$S = S(l,m) = S_l^m(r) Y_l^m(\theta,\phi), \quad \text{and} \quad Y_l^m(\theta,\phi = P_l^m(\cos\theta) e^{im\phi}; \tag{4}$$

where $P_l^m(\cos\theta)$ is the Legendre polynomial. When $l = 1, m = 0$, it corresponds to the dipole mode, i.e.:

$$S(1,0) = C \frac{\cos\theta}{r^2} \sum_{\nu=0}^{\infty} a_\nu (\frac{2M}{r})^\nu,$$
$$a_0 = 1, a_\nu = \frac{(1+\nu)^2 - 1}{(3+\nu)\nu} a_{\nu-1}, \quad (\text{for } \nu \geq 1). \tag{5}$$

From Eqs. (3) to (5), we have the dipole component of the magnetic fields:

$$\mathbf{B}^{surf}(1,0) = \vec{\nabla} \times (\vec{r} \times \vec{\nabla} S(1,0)) = C_1 \cos\theta \frac{1}{r^3} \sum_{\nu=0}^{\infty} a_\nu (\frac{2M}{r})^\nu \vec{e}_r$$
$$+ C_1 \sin\theta \frac{1}{r^3 h} \sum_{\nu=0}^{\infty} (\nu+1) a_\nu (\frac{2M}{r})^\nu \vec{e}_\theta. \tag{6}$$

By working out the summation terms in Eq. (6), a typical form of the magnetar surface magnetic fields (dipole mode) can be obtained [see the field lines in Fig. 1]:

$$\mathbf{B}_{di}^{surf}(1,0) = 2C_1 \cos\theta \frac{1}{r^3} \frac{-3r[r^2 \ln(1 - \frac{2M}{r}) + 2M(M+r)]}{8M^3} \vec{e}_r$$
$$+ C_1 \frac{\sin\theta}{r^3 h} \frac{3r^2[2M(\frac{M}{r-2M} + 1) + r\ln(1 - \frac{2M}{r})]}{4M^3} \vec{e}_\theta, \tag{7}$$

where the metric h is defined as [61]:

$$h = h(r) = (1 - \frac{2M}{r})^{-\frac{1}{2}}, M = \frac{Gm(r)}{c^2}. \tag{8}$$

The $m(r)$ is the mass function to determine the total mass enclosed within sphere of radius r, and $m(r) \equiv$ mass of magnetar in our case since we only concern magnetic fields outside the magnetar. The C_1 and C_2 (see below) are constants that have been calibrated to the values satisfying the strengths of the surface magnetic fields (e.g. 10^{11} T).

Similarly, for $l = 2$, $m = 0$, we have the quadrupole mode of the magnetar surface magnetic fields [see the shape of field in Fig. 2]:

$$\mathbf{B}^{surf}_{quad}(2,0) = 3C_2(3\cos^2\theta - 1)\frac{1}{r^4}\cdot\frac{-3r[r^2\ln(1-\frac{2M}{r})+2M(M+r)]}{8M^3}\vec{e}_r + 3C_2\cos\theta\sin\theta\frac{1}{r^4h}\cdot\frac{3r[2M(\frac{4M^2}{r-2M}+M+r)+r^2\ln(1-\frac{2M}{r})]}{8M^3}\vec{e}_\theta, \quad (9)$$

Magnetar surface magnetic fields in the quadrupole mode would have comparable strength to that in the dipole mode [62]. In dipole mode, the tangential components [$\vec{e}_\theta$ component in Eq. (7)] have the maximum at polar angle $\theta = \pi/2$ [see Fig. 1(a), lower panel], and the radial components [$\vec{e}_r$ component in Eq. (7)] have the maximum around polar angle $\theta = 0$ and π (two magnetic poles). Differently, in quadrupole mode the tangential components [$\vec{e}_\theta$ component in Eq. (9)] have the maximum around $\theta = \pi/4$ and $3\pi/4$ [Fig. 2(a), lower panel], and the maximum of $\vec{e}_r$ component is around $\theta = 0, \pi/2$, and π.

3. Perturbed EM waves caused by the thermal-HFGWs from magnetars

According to previous studies [21–30], interaction between the thermal-HFGWs and the ultra-high surface magnetic fields (presented in the above section), would cause the perturbed EMWs, which could be accumulated during their propagation along with the thermal-HFGWs synchronously due to the identical or almost identical velocities (speed of light) between the GWs and EMWs (accumulation effect). In this section, we will calculate the generation and investigate the characteristic features of such perturbed EMWs.

(i) Perturbed EMWs caused by thermal-HFGWs within a thin layer around the magnetar surface.

We could firstly focus on the perturbed EMWs within a very thin layer. In this case, the thermal-HFGWs could be approximately treated as planar GWs, and the perturbed EMWs will be accumulated only in a very short distance (so the decay of thermal-HFGWs and the surface magnetic fields could be ignored locally). Generally, the metric of such thermal-HFGWs can be written as $g_{\mu\nu} = \eta_{\mu\nu} + h_{\mu\nu}$, where $h_{\mu\nu}$ is a small perturbation to the background spacetime $\eta_{\mu\nu}$, and the non-vanishing component of $h_{\mu\nu}$ should be in the same order of magnitude of the amplitude of the thermal-HFGWs [e.g., $A^{thm}_{+,\times,x,y}$ for tensor and vector modes, Eq. (2)], so we have:

$$g_{\mu\nu} = \eta_{\mu\nu} + h_{\mu\nu} = \begin{pmatrix} -1 & 0 & 0 & 0 \\ 0 & 1 & 0 & 0 \\ 0 & 0 & 1 & 0 \\ 0 & 0 & 0 & 1 \end{pmatrix} + \begin{pmatrix} 0 & 0 & 0 & 0 \\ 0 & A_+ + A_b & A_\times & A_x \\ 0 & A_\times & -A_+ + A_b & A_y \\ 0 & A_x & A_y & \sqrt{2}A_l \end{pmatrix} e^{i(\boldsymbol{k}_g\cdot\boldsymbol{r}-\omega_g t)}, \quad (10)$$

The $(+, \times)$, (x, y) and (b, l) respectively represent the tensor mode, the vector mode, and the scalar mode polarizations (in this article we only include the tensor and vector modes).

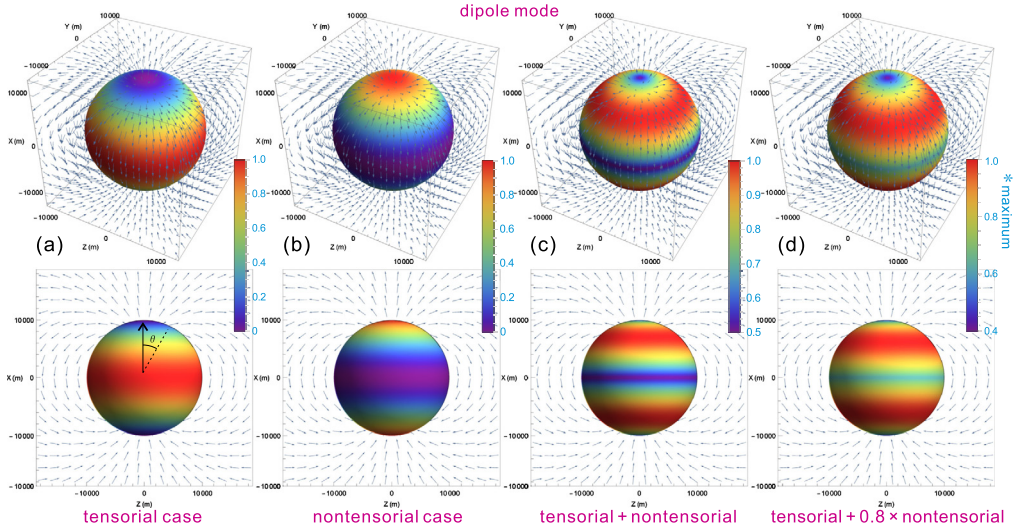

Fig. 1. Perturbed EMWs (in one thin layer) caused by the thermal-HFGWs (from the magnetars) interacting with the ultra-strong surface magnetic fields (in dipole mode) of the magnetars. Sub-figure (a): distribution of the perturbed EMWs around the surface of magnetar, for the case considering tensorial thermal-HFGWs only; the maximum appears around the equator area (polar angle $\theta = \pi/2$) where the tangential components of surface magnetic fields (perpendicular to propagation of thermal-HFGWs, and interacting with the tensorial GWs only) reach their maximum (here we assume the thermal-HFGWs propagating outward isotropically). Sub-figure (b): distribution of the perturbed EMWs for the case considering nontensorial thermal-HFGWs only, and the maximums appear around the two poles where the radial components of surface magnetic fields (along the propagation of thermal-HFGWs, and interacting with the nontensorial GWs only) reach their maximum. Sub-figure (c) and (d): distributions of the perturbed EMWs for the cases having both tensorial and nontensorial thermal-HFGWs in different proportions [e.g. case of (d), $1 \times$ tensorial $+ 0.8 \times$ nontensorial], and their patterns are diverse and different to the cases of (a) and (b). The figures use parameters: magnetar radius $=$ 10 km, Mass $= 3M_{\odot}$, surface magnetic fields $\sim 10^{11}$T, temperature $=$ 4000 Kev. (For interpretation of the colors in the figure (s), the reader is referred to the web version of this article.)

Based on the electrodynamics equations in curved spacetime [16,29]:

$$\begin{aligned}
&\frac{\partial}{\partial x^{\nu}}(\sqrt{-g}g^{\mu\alpha}g^{\nu\beta}F_{\alpha\beta}) = 0,\\
&\nabla_{\mu}F_{\nu\alpha} + \nabla_{\nu}F_{\alpha\mu} + \nabla_{\alpha}F_{\mu\nu} = 0,\\
&\nabla_{\alpha}F_{\mu\nu} = F_{\mu\nu,\alpha} - \Gamma^{\sigma}_{\mu\alpha}F_{\sigma\nu} - \Gamma^{\sigma}_{\nu\alpha}F_{\mu\sigma},
\end{aligned} \tag{11}$$

typical solutions of the perturbed EMWs for this case can be found referring to previous works [16,27,28]:

$$\begin{aligned}
\tilde{E}^{(1)} &= A^{thm}_{+,\times,x,y}\hat{B}^{(0)}_{surf}k^{thm}_{g}c\Delta L\exp[i(\boldsymbol{k}^{thm}_{g}\cdot\boldsymbol{r} - \omega_{g}t)],\\
\tilde{B}^{(1)} &= A^{thm}_{+,\times,x,y}\hat{B}^{(0)}_{surf}k^{thm}_{g}\Delta L\exp[i(\boldsymbol{k}^{thm}_{g}\cdot\boldsymbol{r} - \omega_{g}t)].
\end{aligned} \tag{12}$$

Here, the $A^{thm}_{+,\times,x,y}$ represents dimensionless amplitudes for tensorial or nontensorial thermal-HFGWs; $\hat{B}^{(0)}_{surf}$ is the surface magnetic fields; $\boldsymbol{k}^{thm}_{g}$ is the wave vector of the thermal-HFGWs, and ΔL is the accumulation distance (the distance of interaction of the thermal-HFGW with the strong surface magnetic field). Therefore, the power (P^{thm}_{layer}, averaged, the same hereafter, over receiving surface Δs) of the perturbed EMWs can be given [27]:

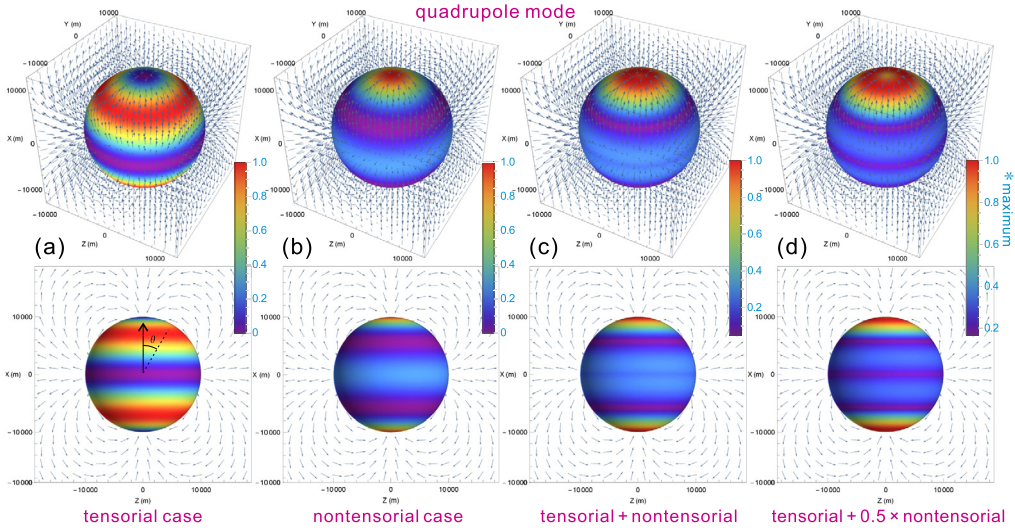

Fig. 2. Perturbed EMWs (in one thin layer) caused by the thermal-HFGWs (from the magnetars) interacting with the ultra-strong surface magnetic fields (in quadrupole mode) of the magnetars. Sub-figure (a): distribution of the perturbed EMWs around the surface of magnetar, for the case considering tensorial thermal-HFGWs only, and the maximum appears around polar angle $\theta = \pi/4$ and $3\pi/4$ where the tangential components of quadrupole-mode surface magnetic fields reach their maximum (different to the dipole mode). Sub-figure (b): distribution of the perturbed EMWs for the case considering nontensorial thermal-HFGWs only, and they concentrate around the two poles and the equator area where the radial components of quadrupole-mode surface magnetic fields reach their peaks. Sub-figure (c) and (d): mixed cases having both tensorial and nontensorial thermal-HFGWs in different proportions, and their patterns are diverse and different to the cases of (a) and (b). The figures use parameters: magnetar radius = 10 km, Mass = $3M_{\odot}$, surface magnetic fields $\sim 10^{11}$T, temperature = 4000 Kev.

$$P^{thm}_{layer} = \frac{1}{2\mu_0}(A^{thm}_{+,\times,x,y}\hat{B}^{(0)}_{surf}k^{thm}_{g}\Delta L)^2 c\Delta s \tag{13}$$

together with Eq. (2), we have:

$$P^{thm}_{layer} = \frac{G P_{total}(\hat{B}^{(0)}_{surf})^2\Delta L^2\Delta s}{\mu_0 c^4 r^2} \tag{14}$$

Here, due to the symmetry of distribution of the thermal-HFGWs sources in the neutron star, we assume the thermal-HFGWs propagate outward isotropically. The concrete distribution of polarizations of the perturbed EMWs (depending on the distribution of polarizations of the thermal-HFGWs) should be complicated, but here we only concern the total energy of these perturbed EMWs including all polarizations, so it will not impact our estimations, and more detailed investigation of the issues about contributions from different polarizations, would be carried out in other separated articles.

However, importantly, the perturbed EMWs are not isotropic. E.g., for the interaction between the tensorial HFGWs and the background magnetic fields, only the tangential component (i.e. the $\vec{e}_\theta$ part of the Eq. (7) or Eq. (9), perpendicular to the propagation direction of thermal-HFGWs) of the surface magnetic fields, will contribute the effect of perturbed EMWs [16,21,27–29], but, for the nontensorial HFGWs, e.g. specifically, for the vector mode GWs (x, y polarizations), only the radial component (along the propagating direction of GWs, i.e. the $\vec{e}_r$ part of Eq. (7) or Eq. (9)) of the surface magnetic fields will contribute the effect of perturbed EMWs [21] (this property

is given by the nonzero terms in the solutions of electrodynamic equations in curved space-time, which can also be obtained by naturally extending the solutions in ref. [29]). Therefore, also due to that such radial or tangential component of surface magnetic fields, has particular strength and distribution with respect to the polar angle θ, the perturbed EMWs around the magnetar surface, would appear in distinct distribution manners, as discussed as follows.

For tensorial cases If consider the dipole mode of the magnetic fields, by the $\vec{e}_\theta$ part of Eq. (7) and Eq. (14), we can have the power density (PD^{di}) of perturbed EMWs around the surface of magnetar (within a thin layer, e.g., $\Delta L = 1$ m here):

$$PD^{di} = 9GP_{total}\sin^2\theta\frac{(C_1[2M(\frac{M}{r-2M}+1)+r\ln(1-\frac{2M}{r})])^2}{16\mu_0 c^4 r^4 h^2 M^6}. \tag{15}$$

The same, for the quadrupole case, together with the $\vec{e}_\theta$ part of Eq. (9), the power density (PD^{quad}) can be obtained:

$$PD^{quad} = 81GP_{total}\cos^2\theta\sin^2\theta\frac{(C_2[2M(\frac{4M^2}{r-2M}+M+r)+r^2\ln(1-\frac{2M}{r})])^2}{64\mu_0 c^4 r^8 h^2 M^6}; \tag{16}$$

For nontensorial cases Different to the tensorial case, for the nontensorial thermal-HFGWs, we only include the radial component of surface magnetic fields for calculation. If consider the dipole mode of surface magnetic fields, by the $\vec{e}_r$ part of Eq. (7) and Eq. (14), we obtain the power density (PD^{di}_{nontsr}, the subscript "nontsr" means nontensorial, the same hereafter) of the perturbed EMWs around the surface of magnetar (within a thin layer, e.g., $\Delta L = 1$ m here):

$$PD^{di}_{nontsr} = 9GP_{total}\cos^2\theta\frac{(C_1[r^2\ln(1-\frac{2M}{r})+2M(M+r)])^2}{16\mu_0 c^4 r^6 M^6}. \tag{17}$$

The same, for the quadrupole mode, together with the $\vec{e}_r$ part of Eq. (9), the power density (PD^{quad}_{nontsr}) can be obtained:

$$PD^{quad}_{nontsr} = 81GP_{total}(3\cos^2\theta-1)^2\frac{(C_2[r^2\ln(1-\frac{2M}{r})+2M(M+r)])^2}{64\mu_0 c^4 r^8 M^6}; \tag{18}$$

Fig. 1 (for dipole mode) and Fig. 2 (for quadrupole mode) present the distributions of power density from the Eqs. (15) to (18), for cases of both tensorial and nontensorial thermal-HFGWs. It is shown that the perturbed EMWs are clearly distributed in diverse manners strongly depending on the form of the surface magnetic fields in dipole or quadrupole modes. In other words, these perturbed EMWs will carry and reflect the information of geometrical structures of the surface magnetic fields.

Specifically, as mentioned above, due to that the tensorial and nontensorial GWs can respectively interact with tangential and radial component of the surface magnetic fields, for the dipole mode and tensorial case, the perturbed EMWs concentrate around $\theta = \pi/2$ ["equator" area, see Fig. 1(a)], where the tangential component of magnetic fields reach the maximum, and differently, for the dipole mode and nontensorial case, the perturbed EMWs reach their maximum around the two poles [Fig. 1(b)]. Whereas, for the mixed cases having both tensorial and nontensorial GWs [Fig. 1(c) and (d)], the distributions present more diverse manners.

Comparatively, for the quadrupole mode, the perturbed EMWs concentrate around $\theta = \pi/4$ and $\theta = 3\pi/4$ for the tensorial case [Fig. 2(a)], and it is in very different pattern for the nontensorial case where three peaks appear [Fig. 2(b)], and further, for the mixed cases they can have

various distinct distributions with even 4 peaks in special angular positions depending on the mixture proportions [Fig. 2(c) and (d)]. Thus, these perturbed EMWs all present very characteristic distributions depending on the structure of the surface magnetic fields and the polarizations of thermal-HFGWs.

(ii) Accumulated perturbed EMWs caused by thermal-HFGWs in the near and far fields area of the magnetars.

Because of the accumulation effect [16,17,20,21,23,24,27–29], the perturbed EMWs would be accumulated during their propagation along with the thermal-HFGWs synchronously in the identical or almost identical speed of light. Interestingly, it had been found that for different forms of GWs and background magnetic fields, the accumulation effect behaves very diversely case to case, but they obey some regular relationships, e.g., through the uniform static background magnetic fields, the planar GWs, the cylindrical GWs and the spherical GWs would lead to accumulated perturbed EMWs with their strengths proportional to $distance^1$ [27–29], $distance^{1/2}$ [24] and $distance^0$ [23], respectively. Hence, for the surface magnetic fields with the form totally different to the background magnetic fields in these previous works, it is an interesting question to investigate how the accumulation effect behaves, for the thermal-HFGWs propagating through this strong-but-nonuniform surface magnetic fields of the magnetars.

For cases of tensorial GWs The generated perturbed EMWs in every thin layer of "dr" (r is along the radial axis) from the magnetar surface ($r = r_0 =$ magnetar radius) to a certain accumulation distance (R, corresponding to the end point of the accumulation we include for calculation) will be accumulated. Referring to Eqs. (2), (7) and (12), the electric component $\tilde{E}^{(1)di}_{accum}$ of the accumulated perturbed EMWs can be integrated (for case of dipole mode of surface magnetic fields):

$$\begin{aligned}\tilde{E}^{(1)di}_{accum} &= \int_{r_0}^{R} |A^{thm}_{+,\times}\hat{B}^{(0)}_{surf}ck^{thm}_g dr|\frac{r}{R} = \int_{r_0}^{R}\sqrt{\frac{P_{total}8\pi G}{4\pi r^2c^3\omega^2}}\\ &\quad\times\frac{\sin\theta C_1}{r^3}\frac{3r^2[2M(\frac{M}{r-2M}+1)+r\ln(1-\frac{2M}{r})]}{4M^3(1-\frac{2M}{r})^{-\frac{1}{2}}}k^{thm}_g c\frac{r}{R}dr\\ &= \frac{\sin\theta C_1}{4M^3R}\sqrt{\frac{8\pi G P_{total}}{4\pi c^3}}\cdot[\Xi_{int}(R)-\Xi_{int}(r_0)];\end{aligned} \tag{19}$$

where,

$$\begin{aligned}\Xi_{int}(r) &= 3\sqrt{1-\frac{2M}{r}}[-2M+r\ln(1-\frac{2M}{r})]\\ &\quad+6M[-\operatorname{arctanh}(\sqrt{1-\frac{2M}{r}})(2+\ln(1-\frac{2M}{r}))\\ &\quad+\ln(-M+r+r\sqrt{1-\frac{2M}{r}})]+12M\sum_{k=1}^{\infty}\frac{(\sqrt{1-\frac{2M}{r}})^k}{k^2}\\ &\quad-3M\sum_{k=1}^{\infty}\frac{(1-\frac{2M}{r})^k}{k^2},\end{aligned} \tag{20}$$

here, $\sum_{k=1}^{\infty}\frac{(\sqrt{1-\frac{2M}{r}})^k}{k^2} = Li_2(\sqrt{1-\frac{2M}{r}})$ is the polylogarithm function of order 2 and argument $\sqrt{1-\frac{2M}{r}}$. The term $\frac{r}{R}$ in the Eq. (19) represents that the electric component of perturbed EMWs will decay into $\frac{r}{R}$ times its value at the position of r, when the perturbed EMW (generated at the position of r) propagates (decaying spherically) and arrives at the distance R (end point of accumulation).

Here, the Eq. (19) is for the situation ideally treating the surface magnetic fields of the magnetars as stationary fields. Actually, the magnetic fields (surface and internal) would be unstable due to complicated reasons and such instability had been long studied [63–72]. There is one case of changing of surface magnetic fields that would be clear and simple, and this change evidently impacts the strengths of perturbed EMWs in some given observational direction, i.e., if the rotational axis and the magnetic axis of the magnetar are misaligned, it will lead to periodic change of the magnetic fields in the line along the observational direction, so the perturbed EMWs will fluctuate in the line of sight with respect to the rotational phase, and then result in particular pulse-like envelopes of the power density or strengths of the perturbed EMWs. E.g., as shown in Fig. 3, β is the angle between rotational and magnetic axes, and ξ is the angle between rotational axis and observational direction (e.g. facing to the Earth), so for the rotation phase $\varphi = \omega t + \varphi_0$, we should add a term of $\eta(\beta, \xi, \omega, \omega_0, t)$ into the Eq. (19) to give the information of this time-dependent effect due to such periodic change of the surface magnetic fields, and then for this tensor-dipole case, the Eq. (19) is modified into:

$$\begin{aligned}
&\tilde{E}^{(1)di}_{accum\text{-}rotate}(t) \\
&\quad = \frac{\eta(\beta,\xi,\omega,\omega_0,t)C_1}{4M^3R}\sqrt{\frac{8\pi G P_{total}}{4\pi c^3}}\cdot[\Xi_{int}(R)-\Xi_{int}(r_0)]; \\
&\qquad \text{where, } \eta(\beta,\xi,\omega,\omega_0,t) = \{\sin^2(\xi)\sin^2(\omega t+\varphi_0) \\
&\quad + [\sin(\beta)\cos(\xi)+\cos(\beta)\sin(\xi)\cos(\omega t+\varphi_0)]^2\}^{\frac{1}{2}}.
\end{aligned} \tag{21}$$

The contribution of term $\eta(\beta, \xi, \omega, \omega_0, t)$ is plotted in subfigure (b) of Fig. 3 for this tensor-dipole case (as an example given particular β and ξ), and for other cases (tensor-quadrupole, etc.), the terms of $\eta(\beta, \xi, \omega, \omega_0, t)$ can be different (see Eqs. below), and the different envelopes they cause, are also presented in other subfigures of the Fig. 3 (it is to be noticed that, in Figs. 1, 2, 4, 5, 6 and Table 2, for clearness, such rotational effect is not presented, or, set the $\beta = 0$).

Similarly, integration of accumulated magnetic component of the perturbed EMWs (also for dipole mode), i.e. the $\tilde{B}^{(1)di}_{accum}$, can be obtained in a similar expression (the only difference is a constant "c", speed of light). Then the power (P^{di}_{accum}, over surface Δs, for the dipole case) of the accumulated perturbed EMWs is:

$$\begin{aligned}
P^{di}_{accum} &= \frac{1}{2\mu_0}|\tilde{E}^{(1)di*}_{accum}\cdot\tilde{B}^{(1)di}_{accum}|\Delta s \\
&= \frac{(\sin\theta C_1)^2 G P_{total}}{16\mu_0 c^4 M^6 R^2}[\Xi_{int}(R)-\Xi_{int}(r_0)]^2.
\end{aligned} \tag{22}$$

For considering the change of surface magnetic fields by rotation, the above P^{di}_{accum} turns into $P^{di}_{accum\text{-}rotate}(t)$:

$$P^{di}_{accum\text{-}rotate}(t) = \frac{1}{2\mu_0}|\tilde{E}^{(1)di*}_{accum}\cdot\tilde{B}^{(1)di}_{accum}|\Delta s$$

Table 2
Maximal power density of the perturbed EMWs in near field area and strengths of magnetic components of the perturbed EMWs in far field area, caused by interaction between the thermal-HFGWs and the ultra-strong surface magnetic fields of the magnetars. Here, "dipole, tensorial" means the case of tensorial thermal-HFGWs interacting with dipole mode surface magnetic fields. The "quad." means quadrupole mode.

Assumed possible magnetar radius and mass	Temperature of thermal source	Thermal HFGW freq. (Hz)	Total power of thermal HFGW (W)	PD^{max} = maximum of power density (Watt/m^2) of perturbed EMWs in near field, r_{max} = position (km) of the maximum in near field, $\tilde{B}^{far}_{ptbd}$ = magnetic component (Gauss) of perturbed EMWs in far field ($\sim 10^{19}$ m).			
				dipole, tensorial $PD^{max}\|r_{max}\|\tilde{B}^{far}_{ptbd}$	dipole, nontensorial $PD^{max}\|r_{max}\|\tilde{B}^{far}_{ptbd}$	quad., tensorial $PD^{max}\|r_{max}\|\tilde{B}^{far}_{ptbd}$	quad., nontensorial $PD^{max}\|r_{max}\|\tilde{B}^{far}_{ptbd}$
12 km	8k Kev	1.9E21	6.7E24	1.3E8|20.0|3.0E-14	2.2E8|20.2|4.0E-14	9.4E7|18.7|2.2E-14	1.5E8|18.7|2.8E-14
$1.6M_\odot$	4k Kev	9.7E20	4.2E23	8.0E6|20.0|7.5E-15	1.4E7|20.2|1.0E-14	5.8E6|18.7|5.5E-15	9.5E6|18.7|6.9E-15
13 km	8k Kev	1.9E21	8.3E24	1.4E8|21.5|3.3E-14	2.6E8|21.7|4.7E-14	1.0E8|20.2|2.4E-14	1.8E8|20.1|3.3E-14
$2M_\odot$	4k Kev	9.7E20	5.2E23	8.4E6|21.5|8.3E-15	1.7E7|21.7|1.2E-14	6.3E6|20.2|6.1E-15	1.1E7|20.1|8.2E-15
10 km	8k Kev	1.9E21	1.2E25	1.5E8|16.4|2.7E-14	3.6E8|16.6|4.2E-14	1.2E8|15.4|2.0E-14	2.5E8|15.4|2.9E-14
$1.8M_\odot$	4k Kev	9.7E20	7.3E23	9.6E6|16.4|6.7E-15	2.2E7|16.6|1.0E-14	7.3E6|15.4|5.0E-15	1.5E7|15.4|7.2E-15

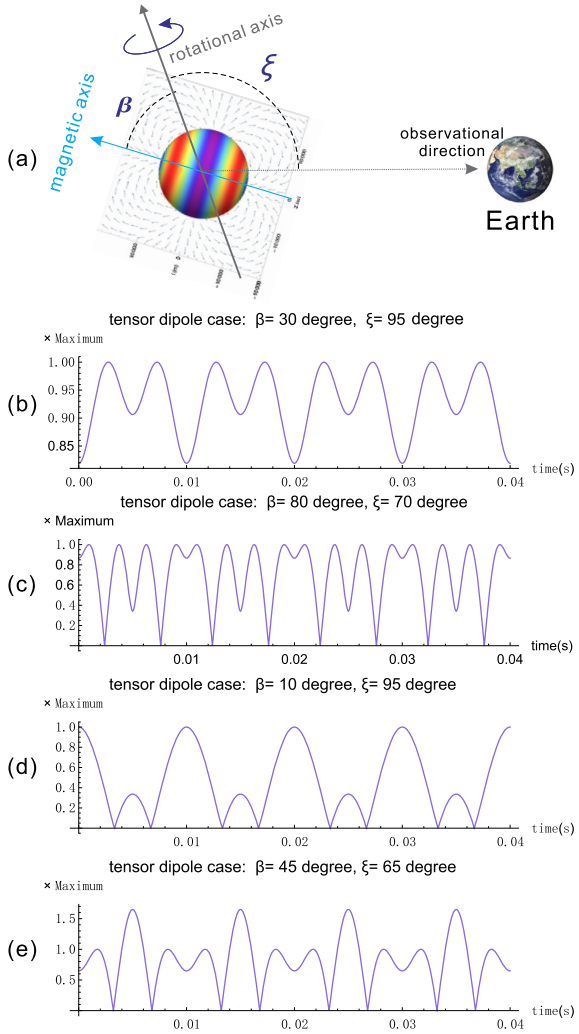

Fig. 3. (a) Misalignment of rotational and magnetic axes leads to changing of magnetic fields along given observational direction and thus results in particular envelopes of electric components of perturbed EMWs in line of sight; β is the angle between rotational and magnetic axes, and ξ is the angle between rotational axis and observational direction. (b) to (e), example envelopes for tensor-dipole case, tensor-quadrupole case, nontensor-dipole case and nontensor-quadrupole case, respectively. Here ω and φ_0 are set to 100 Hz $\cdot 2\pi$ and 0.

$$= \frac{\eta(\beta,\xi,\omega,\omega_0,t)(C_1)^2 G P_{total}}{16\mu_0 c^4 M^6 R^2}[\Xi_{int}(R) - \Xi_{int}(r_0)]^2;$$

$$\text{where, } \eta(\beta,\xi,\omega,\omega_0,t) = \sin^2(\xi)\sin^2(\omega t+\varphi_0) + [\sin(\beta)\cos(\xi)+\cos(\beta)\sin(\xi)\cos(\omega t+\varphi_0)]^2 \tag{23}$$

The same, referring to Eqs. (2), (9) and (12), the accumulated electric component of perturbed EMWs of the surface magnetic fields (in quadrupole mode) can be obtained:

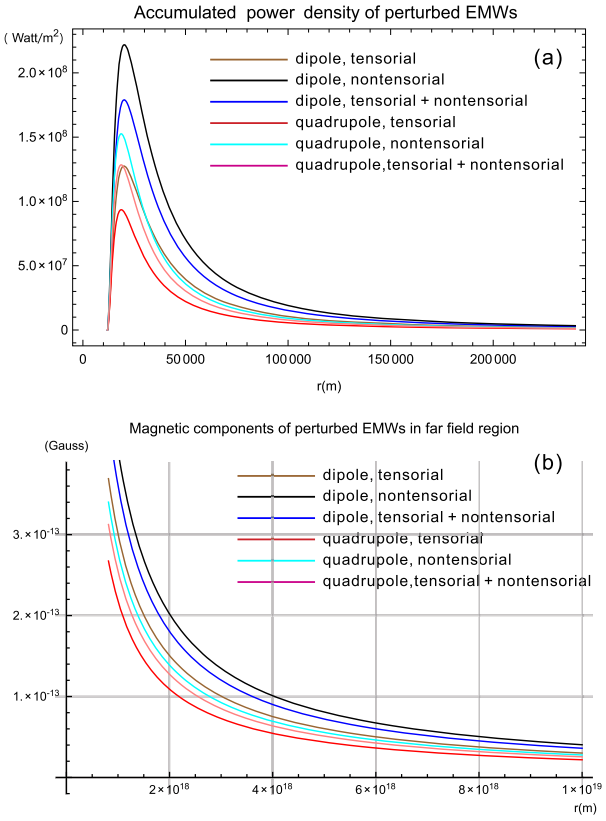

Fig. 4. (a) accumulated power density of the perturbed EMWs in near field area, and (b) strengths of magnetic components of the perturbed EMWs in far field area, caused by the thermal-HFGWs (from magnetars) interacting with the ultra-strong magnetar surface magnetic fields. Here, magnetar radius = 12 km and magnetar mass = $1.6M_{\odot}$. The curves are from Eqs. (19) to (34).

$$\begin{aligned}\tilde{E}^{(1)quad}_{accum} &= \int_{r_0}^{R} |A_{+,\times}\hat{B}^{(0)}_{surf} c k_g^{thm} dr| \frac{r}{R} \\ &= \int_{r_0}^{R} \sqrt{\frac{P_{total} 8\pi G}{4\pi r^2 c^3 \omega^2}} \cdot \frac{3C_2 |\sin\theta\cos\theta|}{r^4} \\ &\quad \times \frac{3r[2M(\frac{4M^2}{r-2M} + M + r) + r^2 \ln(1-\frac{2M}{r})]}{8M^3(1-\frac{2M}{r})^{-\frac{1}{2}}} k_g^{thm} c \frac{r}{R} dr \\ &= \frac{3C_2|\sin\theta\cos\theta|}{40M^3R^3} \sqrt{\frac{8\pi G P_{total}}{4\pi c^3}} \cdot [\Xi^{qua}_{int}(R) - \Xi^{qua}_{int}(r_0)]; \end{aligned} \tag{24}$$

where,

$$\Xi^{qua}_{int}(r) = 30r^2 \operatorname{arctanh}(\sqrt{1-\frac{2M}{r}}) \ln(1-\frac{2M}{r})$$

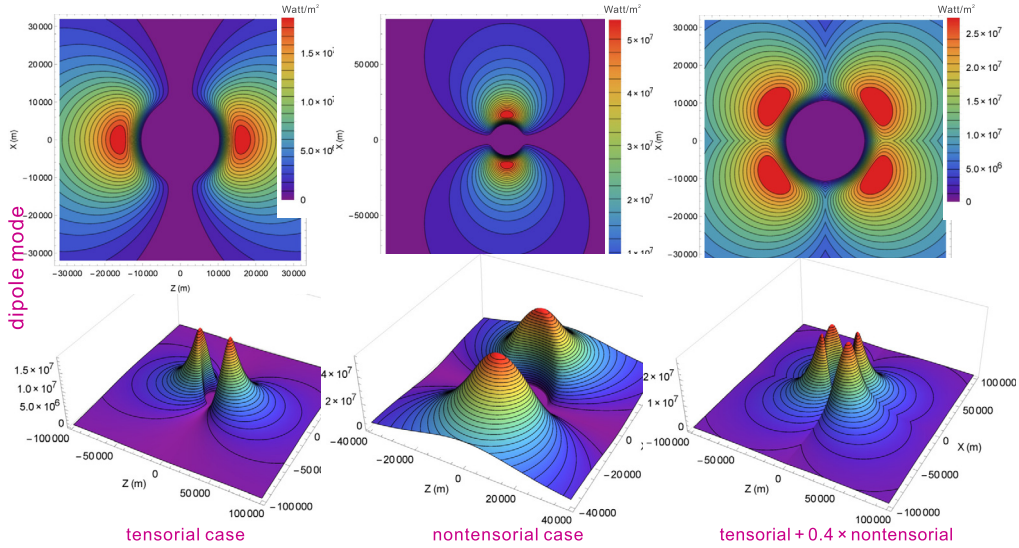

Fig. 5. Accumulated perturbed EMWs caused by magnetar thermal-HFGWs in dipole-mode surface magnetic fields. Sub-figure (a) shows the power density (Wm^{-2}) of perturbed EMWs accumulated from the magnetar surface to several magnetar radii for the case having only tensorial GWs, and it reaches the maximums around 1.5 magnetar radius. Sub-figure (b) presents the case having only nontensorial GWs, and the direction is perpendicular to the case (a). Sub-figure (c) shows the case having both tensorial and nontensorial GWs with a certain proportion. Different cases present various characteristic manners of the perturbed EMWs. Figures are generated from Eqs. (19) to (22), (29) and (33), with typical parameters: magnetar radius ~ 10 km, magnetar mass $\sim 3M_{\odot}$, maximum of magnetar surface magnetic fields $\sim 10^{11}$ T, temperature of thermal source of HFGWs ~ 4000 keV.

$$
\begin{aligned}
&-2\sqrt{1-\frac{2M}{r}}[-6M^2+Mr-44r^2+15r^2\ln(1-\frac{2M}{r})]\\
&+15r^2(\sum_{k=1}^{\infty}\frac{(1-\frac{2M}{r})^k}{k^2}-4\sum_{k=1}^{\infty}\frac{(\sqrt{1-\frac{2M}{r}})^k}{k^2}).
\end{aligned}
\tag{25}
$$

For considering the rotation, the above $\tilde{E}^{(1)quad}_{accum}$ becomes $\tilde{E}^{(1)quad}_{accum\text{-}rotate}(t)$:

$$
\begin{aligned}
\tilde{E}^{(1)quad}_{accum\text{-}rotate}(t) = &\frac{\eta(\beta,\xi,\omega,\omega_0,t)3C_2}{40M^3R^3}\sqrt{\frac{8\pi G P_{total}}{4\pi c^3}}\cdot[\Xi^{qua}_{int}(R)-\Xi^{qua}_{int}(r_0)];\\
&\text{where, } \eta(\beta,\xi,\omega,\omega_0,t)=\\
&|\cos(\beta)\cos(\xi)-\sin(\beta)\sin(\xi)\cos(\omega t+\varphi_0)|\\
&\times\{[\sin(\beta)\cos(\xi)+\cos(\beta)\sin(\xi)\cos(\omega t+\varphi_0)]^2\\
&+\sin^2(\xi)\sin^2(\omega t+\varphi_0)\}^{\frac{1}{2}}
\end{aligned}
\tag{26}
$$

then the power P^{quad}_{accum} (for the quadrupole case) of the accumulated perturbed EMWs is:

$$
\begin{aligned}
P^{quad}_{accum} &= \frac{1}{2\mu_0}|\tilde{E}^{(1)quad*}_{accum}\cdot\tilde{B}^{(1)quad}_{accum}|\Delta s\\
&= \frac{(\frac{3}{2}C_2\sin\theta\cos\theta)^2 G P_{total}}{400\mu_0 c^4 M^6 R^2}[\Xi^{qua}_{int}(R)-\Xi^{qua}_{int}(r_0)]^2;
\end{aligned}
\tag{27}
$$

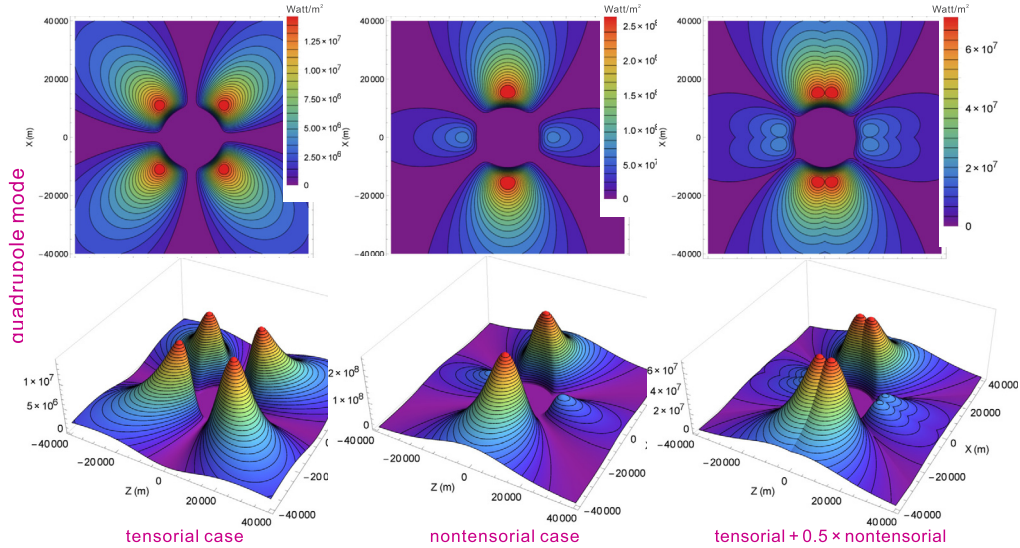

Fig. 6. Accumulated perturbed EMWs caused by magnetars thermal-HFGWs in quadrupole-mode surface magnetic fields. Sub-figure (a) shows the power density ($\mathrm{W\,m^{-2}}$) of perturbed EMWs accumulated from magnetar surface to several magnetar radii for the case having only tensorial GWs. Sub-figure (b) presents the case having only nontensorial GWs. Sub-figure (c) shows the case having both tensorial and nontensorial GWs with a certain proportion. Different cases present various very unique patterns of the perturbed EMWs. Figures are generated from Eqs. (24) to (27), (31) and (34), with typical parameters: magnetar radius ~ 10 Km, magnetar mass $\sim 3M_{\odot}$, maximum of magnetar surface magnetic fields $\sim 10^{11}$ T, temperature of thermal source of HFGWs ~ 4000 keV.

For considering the rotation, the above P^{quad}_{accum} is modified into $P^{quad}_{accum\text{-}rotate}(t)$:

$$
\begin{aligned}
P^{quad}_{accum\text{-}rotate} &= \frac{\eta(\beta,\xi,\omega,\omega_0,t)(\frac{3}{2}C_2)^2 G P_{total}}{400\mu_0 c^4 M^6 R^2}[\Xi^{qua}_{int}(R) - \Xi^{qua}_{int}(r_0)]^2; \\
&\text{where, } \eta(\beta,\xi,\omega,\omega_0,t) = \{[\sin(\beta)\cos(\xi) \\
&+ \cos(\beta)\sin(\xi)\cos(\omega t+\varphi_0)]^2 + \sin^2(\xi)\sin^2(\omega t+\varphi_0)\} \\
&\times [\cos(\beta)\cos(\xi) - \sin(\beta)\sin(\xi)\cos(\omega t+\varphi_0)]^2
\end{aligned} \tag{28}
$$

For cases of nontensorial GWs Only the radial component of the surface magnetic fields is included for calculation, and following similar calculation, referring to Eqs. (2), (7), (9) and (12), the electric component $\tilde{E}^{(1)di\text{-}nontsr}_{accumulation}$ (dipole mode) of the accumulated perturbed EMWs is worked out:

$$
\begin{aligned}
\tilde{E}^{(1)di\text{-}nontsr}_{accumulation} &= \int_{r_0}^{R} |A_{x,y}\hat{B}^{(0)}_{surf} c k^{thm}_g dr| \frac{r}{R} = \int_{r_0}^{R} \sqrt{\frac{P_{total} 8\pi G}{4\pi r^2 c^3 \omega^2}} \\
&\times 2C_1 |\cos\theta| \frac{1}{r^3} \frac{-3r[r^2 \ln(1-\frac{2M}{r}) + 2M(M+r)]}{8M^3} k^{thm}_g c \frac{r}{R} dr \\
&= \frac{2C_1|\cos\theta|}{8M^3R^2r_0}\sqrt{\frac{8\pi G P_{total}}{4\pi c^3}} \cdot \{6M^2(r_0 - R)
\end{aligned}
$$

$$+3Rr_0[-R\ln(1-\frac{2M}{R})+r_0\ln(1-\frac{2M}{r_0})$$
$$+2M\ln\frac{Rr_0-2Mr_0}{Rr_0-2MR}]\};\tag{29}$$

For considering the change of surface magnetic by rotation, the above $\tilde{E}^{(1)di\text{-}nontsr}_{accumulation}$ turns into $\tilde{E}^{(1)di\text{-}nontsr}_{accum\text{-}rotate}(t)$:

$$\tilde{E}^{(1)di\text{-}nontsr}_{accum\text{-}rotate}(t)=\frac{\eta(\beta,\xi,\omega,\omega_0,t)2C_1}{8M^3R^2r_0}\sqrt{\frac{8\pi GP_{total}}{4\pi c^3}}\cdot\{6M^2(r_0-R)$$
$$+3Rr_0[-R\ln(1-\frac{2M}{R})+r_0\ln(1-\frac{2M}{r_0})+2M\ln\frac{Rr_0-2Mr_0}{Rr_0-2MR}]\};$$
$$\text{where, }\ \eta(\beta,\xi,\omega,\omega_0,t)=$$
$$|\cos(\beta)\cos(\xi)-\sin(\beta)\sin(\xi)\cos(\omega t+\varphi_0)|\tag{30}$$

and the electric component $\tilde{E}^{(1)quad\text{-}nontsr}_{accumulation}$ (for quadrupole mode of surface magnetic fields) of the accumulated perturbed EMWs is obtained:

$$\tilde{E}^{(1)quad\text{-}nontsr}_{accumulation}=\int_{r_0}^{R}|A_{x,y}\hat{B}^{(0)}_{surf}ck_g^{thm}dr|\frac{r}{R}$$
$$=\int_{r_0}^{R}\sqrt{\frac{P_{total}8\pi G}{4\pi r^2c^3\omega^2}}\cdot 3C_2|3\cos^2\theta-1|\frac{1}{r^4}$$
$$\cdot\frac{-3r[r^2\ln(1-\frac{2M}{r})+2M(M+r)]}{8M^3}k_g^{thm}c\frac{r}{R}dr$$
$$=\frac{3C_2|3\cos^2\theta-1|}{8M^3R^3r_0^2}\sqrt{\frac{8\pi GP_{total}}{4\pi c^3}}$$
$$\cdot[-3M(R-r_0)(2Rr_0+MR+Mr_0)$$
$$+3R^2r_0^2(\sum_{k=1}^{\infty}\frac{(2M/r_0)^k}{k^2}-\sum_{k=1}^{\infty}\frac{(2M/R)^k}{k^2})];\tag{31}$$

For considering the change of surface magnetic by rotation, the above $\tilde{E}^{(1)quad\text{-}nontsr}_{accumulation}$ becomes $\tilde{E}^{(1)quad\text{-}nontsr}_{accum\text{-}rotate}(t)$:

$$\tilde{E}^{(1)quad\text{-}nontsr}_{accum\text{-}rotate}(t)=\frac{\eta(\beta,\xi,\omega,\omega_0,t)3C_2}{8M^3R^3r_0^2}\sqrt{\frac{8\pi GP_{total}}{4\pi c^3}}$$
$$\cdot[-3M(R-r_0)(2Rr_0+MR+Mr_0)$$
$$+3R^2r_0^2(\sum_{k=1}^{\infty}\frac{(2M/r_0)^k}{k^2}-\sum_{k=1}^{\infty}\frac{(2M/R)^k}{k^2})$$
$$\text{where, }\ \eta(\beta,\xi,\omega,\omega_0,t)=$$
$$\frac{1}{8}|(3\cos(2\beta)+1)(3\cos(2\xi)+1)$$

$$+ 12\sin^2(\beta)\sin^2(\xi)\cos[(2(\omega t+\varphi_0)] - 12\sin(2\beta)\sin(2\xi)\cos(\omega t+\varphi_0)| \tag{32}$$

Therefore, in the cases of nontensorial GWs, the power ($P_{accum}^{di\text{-}nontsr}$, over receiving surface Δs) for the dipole mode and the power ($P_{accum}^{quad\text{-}nontsr}$) for the quadrupole mode of the accumulated perturbed EMWs are as follows respectively:

$$P_{accumulation}^{di\text{-}nontsr} = \frac{1}{2\mu_0 c}|\tilde{E}_{accumulation}^{(1)di\text{-}nontsr}|^2\Delta s, \tag{33}$$

and

$$P_{accumulation}^{quad\text{-}nontsr} = \frac{1}{2\mu_0 c}|\tilde{E}_{accumulation}^{(1)quad\text{-}nontsr}|^2\Delta s. \tag{34}$$

The Table 2 presents the maximal power density of the perturbed EMWs in near field area and the strengths of magnetic components of perturbed EMWs in far field area, according to Eqs. (19) to (34) for various cases including tensorial and nontensorial GWs in dipole or quadrupole surface magnetic fields of magnetars, given various typical parameters. For the safe estimations, the numerical results in Table 2 only take the accumulation effect from the magnetar surface to 10^7 m into account, and drop the contributions after this distance. We find the power density of the perturbed EMWs would reach $\sim 10^6 - 10^8$ W/m^2 in the near field area. Such EMWs could also be actually a sort of interesting EM counterparts of the thermal GWs, and these weak EMWs (or with higher strengths caused by some possible closer sources) perhaps would be captured in the foreseeable future by very fast developing techniques of sensitive EM wave detectors. However, we here only try to reveal a potential novel effect of the perturbed EMWs, and the concrete observational technique is not the key concern in this article and it shall be investigated in detail elsewhere. In Table 2, we can also find that the configurations of magnetars (mass and radius) bring a non-linear influence to either the frequency-amplitude of the thermal-HFGWs or the strengths of perturbed EMWs.

Fig. 4 presents the curves of accumulated power density of the perturbed EMWs in near field area, and the strengths of magnetic components of the perturbed EMWs in far field area. These curves are consistent to the results shown in the Table 2, and these behaviors of perturbed EMWs for various cases are generally accordant to each other. Figs. 5 and 6 [produced from Eqs. (19) to (34)] present very distinctive and unique distributions of the perturbed EMWs for the dipole and quadrupole modes respectively, including cases having tensorial GWs, nontensorial GWs and both.

In brief, the perturbed EMWs would have very characteristic distributions depending on the magnetar structures and the crucial information of the tensorial and possible nontensorial polarizations of the thermal-HFGWs from the magnetars.

4. Summary and discussion

Considering the magnetars as the natural astrophysical laboratories providing extremely strong celestial EM environments, this article try to predict the novel effect of the perturbed EMWs with distinctive patterns caused by the tensorial and possible nontensorial thermal-HFGWs (from the thermal sources of gravitational bremsstrahlung in magnetars) interacting with the ultra-strong surface magnetic fields of the magnetars.

Specifically, we have the summary:

1. The analytical expressions of the perturbed EMWs caused by the thermal-HFGWs from the magnetars, have been obtained [Eqs. (19) to (34)], and their levels are predicted (Table 2 and Figs. 4 to 6, by typical parameters). The power density of the perturbed EMWs would reach $\sim 10^6$–10^8 W/m^2 in the near field area (Table 2), and due to the rotation of magnetars, the strengths of perturbed EMWs in the observational direction would appear in characteristic pulse-like envelopes (Fig. 3). Such perturbed EMWs could also be a sort of interesting EM counterparts of the thermal GWs.

2. The perturbed EMWs caused by the thermal-HFGWs would have very characteristic patterns (Figs. 1, 2, 5 and 6) for different cases of dipole or quadrupole surface magnetic fields and the tensorial or possible nontensorial thermal-HFGWs. Such distinctive patterns from the magnetars had never been predicted before, which may deliver and reflect the particular geometrical information of the surface magnetic fields and the crucial features of the GW polarizations. Thus, they would be potential evidences of the possible nontensorial GWs, the thermal-HFGWs from the magnetars, the mechanism of EM response to the GWs, the models of magnetars and their magnetic fields.

We here only focus on the dipole and quadrupole modes of the magnetar surface magnetic fields. Actually, several other models had also been proposed with different configurations of the magnetar magnetospheres, e.g., some of them suggest the twisted dipole [73] instead of a centred dipole, the higher multiple components [74], and some other more complicated structures [75, 76]. Therefore, related works for diverse patterns of the perturbed EMWs based on alternative magnetar structures, would also be interesting topics.

Acknowledgements

This project is supported by National Natural Science Foundation of China (Grant No. 11605015, No. 11375279, No. 11873001, No. 11847301), Fundamental Research Funds for the Central Universities (2019CDXYWL0029), Science and Technology Research Program of Chongqing Municipal Education Commission (Grant No. KJQN201800105), Natural Science Foundation Project of Chongqing cstc2018jcyjAX0767.

References

[1] B.P. Abbott, et al., LIGO Scientific Collaboration, Virgo Collaboration, Phys. Rev. Lett. 116 (2016) 061102.
[2] B.P. Abbott, et al., LIGO Scientific Collaboration, Virgo Collaboration, Phys. Rev. Lett. 116 (2016) 241103.
[3] B.P. Abbott, et al., LIGO Scientific Collaboration, Virgo Collaboration, Phys. Rev. Lett. 118 (2017) 221101.
[4] B.P. Abbott, et al., Astrophys. J. Lett. 851 (2017) L35.
[5] B.P. Abbott, et al., LIGO Scientific Collaboration, Virgo Collaboration, Phys. Rev. Lett. 119 (2017) 141101.
[6] B.P. Abbott, et al., LIGO Scientific Collaboration, Virgo Collaboration, Phys. Rev. Lett. 119 (2017) 161101.
[7] B.P. Abbott, et al., LIGO Scientific Collaboration, Virgo Collaboration, arXiv:1811.12907 [astro-ph.HE].
[8] B.P. Abbott, et al., LIGO Scientific Collaboration, Virgo Collaboration, Phys. Rev. X 6 (2016) 041015.
[9] P.A.R. Ade, Y. Akiba, A.E. Anthony, K. Arnold, M. Atlas, et al., Phys. Rev. Lett. 113 (2014) 021301.
[10] D. Baskaran, L.P. Grishchuk, A.G. Polnarev, Phys. Rev. D 74 (2006) 083008.
[11] U. Seljak, M. Zaldarriaga, Phys. Rev. Lett. 78 (1997) 2054.
[12] J.R. Pritchard, M. Kamionkowski, Ann. Phys. (N.Y.) 318 (2005) 2.
[13] W. Zhao, Y. Zhang, Phys. Rev. D 74 (2006) 083006.
[14] Z. Chang, C.-G. Huang, Z.-C. Zhao, Chin. Phys. C 41 (2017) 093108.
[15] V.B. Braginsky, L.P. Grishchuk, A.G. Doroshkevich, Y.B. Zeldovich, I.D. Novikov, M.V. Sazhin, Zh. Èksp. Teor. Fiz. 65 (1973) 1729.
[16] D. Boccaletti, V. De Sabbata, P. Fortint, C. Gualdi, Nuovo Cimento B 70 (1970) 129.
[17] W.K. De Logi, A.R. Mickelson, Phys. Rev. D 16 (1977) 2915.

[18] P. Chen, Phys. Rev. Lett. 74 (1995) 634.
[19] P. Chen, Stanford Linear Accelerator Center Report (SLAC-PUB-6666), 1994, p. 379.
[20] H.N. Long, D.V. Soa, T.A. Tuan, Phys. Lett. A 186 (1994) 382.
[21] F.Y. Li, H. Wen, Z.Y. Fang, D. Li, T.J. Zhang, arXiv:1712.00766 [gr-qc], 2018.
[22] F.Y. Li, H. Wen, Z.Y. Fang, L.F. Wei, Y.W. Wang, M. Zhang, Nucl. Phys. B 911 (2016) 500.
[23] H. Wen, F.Y. Li, Z.Y. Fang, Phys. Rev. D 89 (2014) 104025.
[24] H. Wen, F.Y. Li, Z.Y. Fang, A. Beckwith, Eur. Phys. J. C 74 (2014) 2998.
[25] F.Y. Li, H. Wen, Z.Y. Fang, Chin. Phys. B 22 (2013) 120402.
[26] J. Li, K. Lin, F.Y. Li, Y.H. Zhong, Gen. Relativ. Gravit. 43 (2011) 2209.
[27] F.Y. Li, N. Yang, Z.Y. Fang, R.M.L. Baker, G.V. Stephenson, H. Wen, Phys. Rev. D 80 (2009) 064013.
[28] F.Y. Li, R.M.L. Baker Jr., Z.Y. Fang, G.V. Stepheson, Z.Y. Chen, Eur. Phys. J. C 56 (2008) 407.
[29] F.Y. Li, M.X. Tang, D.P. Shi, Phys. Rev. D 67 (2003) 104008.
[30] F.Y. Li, M.X. Tang, J. Luo, Y.C. Li, Phys. Rev. D 62 (2000) 044018.
[31] X. Li, S. Wang, H. Wen, Chin. Phys. C 40 (2016) 085101.
[32] G. Schäfer, H. Dehnen, Phys. Rev. D 27 (1983) 2864.
[33] G. Schäfer, H. Dehnen, Phys. Rev. D 23 (1981) 2129.
[34] F. Romero, H. Dehnen, Astrophys. Space Sci. 89 (1983) 115.
[35] H. Dehnen, F. Ghaboussi, Class. Quantum Gravity 2 (1985) L141.
[36] H. Dehnen, F. Romero, G. Schafer, Class. Quantum Gravity 1 (1984) 305.
[37] G. Papini, S. Valluri, Phys. Rep. 33 (1977) 51.
[38] S. del Campo, L.H. Ford, Phys. Rev. D 38 (1988) 3657.
[39] R.J. Gould, Astrophys. J. 288 (1985) 789.
[40] D.M. Eardley, D.L. Lee, A.P. Lightman, R.V. Wagoner, C.M. Will, Phys. Rev. Lett. 30 (1973) 884.
[41] D.M. Eardley, D.L. Lee, A.P. Lightman, Phys. Rev. D 8 (1973) 3308.
[42] C. Brans, R.H. Dicke, Phys. Rev. 124 (1961) 925.
[43] Y. Fujii, K. Maeda, The Scalar-Tensor Theory of Gravitation, Cambridge University Press, Cambridge, England, 2002.
[44] C. de Rham, L. Heisenberg, Phys. Rev. D 84 (2011) 043503.
[45] L. Heisenberg, R. Kimura, K. Yamamoto, Phys. Rev. D 89 (2014) 103008.
[46] J.B. Jiménez, L. Heisenberg, Phys. Lett. B 757 (2016) 405.
[47] S. Capozziello, M. Francaviglia, Gen. Relativ. Gravit. 40 (2008) 357.
[48] G. Dvali, G. Gabadadze, M. Porrati, Phys. Lett. B 485 (2000) 208.
[49] S.S. Seahra, C. Clarkson, R. Maartens, Phys. Rev. Lett. 94 (2005) 121302.
[50] C. Clarkson, S.S. Seahra, Class. Quantum Gravity 24 (2007) F33.
[51] D. Andriot, G.L. Gómez, J. Cosmol. Astropart. Phys. 2017 (2017) 048.
[52] H. Takeda, A. Nishizawa, Y. Michimura, K. Nagano, K. Komori, M. Ando, K. Hayama, Phys. Rev. D 98 (2018) 022008.
[53] B.P. Abbott, et al., LIGO Scientific Collaboration, Virgo Collaboration, Phys. Rev. Lett. 120 (2018) 031104.
[54] M. Isi, A.J. Weinstein, arXiv:1710.03794 [gr-qc], 2017.
[55] K. Chatziioannou, N. Yunes, N. Cornish, Phys. Rev. D 86 (2012) 022004.
[56] J.D. Bekenstein, Phys. Rev. D 70 (2004) 083509.
[57] N. Yunes, F. Pretorius, Phys. Rev. D 80 (2009) 122003.
[58] N. Cornish, L. Sampson, N. Yunes, F. Pretorius, Phys. Rev. D 84 (2011) 062003.
[59] L.D. Landau, E.M. Lifshitz, The Classical Theory of Fields, Nauka, Moscow, 1973, pp. 368–370.
[60] B.D. Metzger, T.A. Thompson, E. Quataert, Astrophys. J. 659 (2007) 561.
[61] K.-H. Rädler, H. Fuchs, U. Geppert, M. Rheinhardt, T. Zannias, Phys. Rev. D 64 (2001) 083008.
[62] C. Thompson, Astrophys. J. 688 (2008) 1258.
[63] K.H. Prendergast, Astrophys. J. 123 (1956) 498.
[64] R.J. Tayler, Mon. Not. R. Astron. Soc. 161 (1973) 365.
[65] R. Arlt, G. Rüdiger, Proc. Int. Astron. Union 6 (2010) 213.
[66] G.A.E. Wright, Mon. Not. R. Astron. Soc. 162 (1973) 339.
[67] R.C. Duncan, C. Thompson, Astrophys. J. Lett. 392 (1992) L9.
[68] M. Goossens, R.J. Tayler, Mon. Not. R. Astron. Soc. 193 (1980) 833.
[69] T. Akgün, I. Wasserman, Mon. Not. R. Astron. Soc. 383 (2008) 1551.
[70] T. Akgün, A. Reisenegger, A. Mastrano, P. Marchant, Mon. Not. R. Astron. Soc. 433 (2013) 2445.
[71] S. Dall'Osso, J. Granot, T. Piran, Mon. Not. R. Astron. Soc. 422 (2012) 2878.

[72] R. Ciolfi, V. Ferrari, L. Gualtieri, J.A. Pons, Mon. Not. R. Astron. Soc. 397 (2009) 913.
[73] C. Thompson, M. Lyutikov, S.R. Kulkarni, Astrophys. J. 574 (2002) 332.
[74] L. Pavan, R. Turolla, S. Zane, L. Nobili, Mon. Not. R. Astron. Soc. 395 (2009) 753.
[75] S. Zane, R. Turolla, Mon. Not. R. Astron. Soc. 366 (2006) 727.
[76] M. Ruderman, Astrophys. J. 382 (1991) 576.